The structure of ionic aqueous solutions at interfaces: An intrinsic structure analysis

Fernando Bresme, Enrique Chacón, Pedro Tarazona, and Aaron Wynveen

Citation: J. Chem. Phys. **137**, 114706 (2012); doi: 10.1063/1.4753986
View online: http://dx.doi.org/10.1063/1.4753986
View Table of Contents: http://jcp.aip.org/resource/1/JCPSA6/v137/i11
Published by the American Institute of Physics.

Additional information on J. Chem. Phys.

Journal Homepage: http://jcp.aip.org/
Journal Information: http://jcp.aip.org/about/about_the_journal
Top downloads: http://jcp.aip.org/features/most_downloaded
Information for Authors: http://jcp.aip.org/authors

ADVERTISEMENT

Downloaded 12 Dec 2012 to 128.101.221.90. Redistribution subject to AIP license or copyright; see http://jcp.aip.org/about/rights_and_permissions

The structure of ionic aqueous solutions at interfaces: An intrinsic structure analysis

Fernando Bresme,[1,2,a)] Enrique Chacón,[3,4,b)] Pedro Tarazona,[4,5,c)] and Aaron Wynveen[6,d)]
[1]*Department of Chemistry, Imperial College London, London SW7 2AZ, United Kingdom*
[2]*Department of Chemistry, Norwegian University of Science and Technology, Trondheim, Norway*
[3]*Instituto de Ciencia de Materiales de Madrid, CSIC, 28049 Madrid, Spain*
[4]*Instituto de Ciencia de Materiales Nicolaś Cabrera, Universidad Autońoma de Madrid, Madrid 28049, Spain*
[5]*Departamento de Física Teórica de la Materia Condensada, Universidad Autońoma de Madrid, Madrid 28049, Spain*
[6]*School of Physics and Astronomy, University of Minnesota, Minneapolis, Minnesota 55455, USA*

(Received 23 June 2012; accepted 5 September 2012; published online 20 September 2012)

We investigate the interfacial structure of ionic solutions consisting of alkali halide ions in water at concentrations in the range 0.2–1.0 molal and at 300 K. Combining molecular dynamics simulations of point charge ion models and a recently introduced computational approach that removes the averaging effect of interfacial capillary waves, we compute the intrinsic structure of the aqueous interface. The interfacial structure is more complex than previously inferred from the analysis of mean profiles. We find a strong alternating double layer structure near the interface, which depends on the cation and anion size. Relatively small changes in the ion diameter disrupt the double layer structure, promoting the adsorption of anions or inducing the density enhancement of small cations with diameters used in simulation studies of lithium solutions. The density enhancement of the small cations is mediated by their strong water solvation shell, with one or more water molecules "anchoring" the ion to the outermost water layer. We find that the intrinsic interfacial electrostatic potential features very strong oscillations with a minimum at the liquid surface that is ∼4 times stronger than the electrostatic potential in the bulk. For the water model employed in this work, SPC/E, the electrostatic potential at the water surface is ∼−2 V, equivalent to ∼80 k_BT (for $T = 300$ K), much stronger than previously considered. Furthermore, we show that the utilization of the intrinsic surface technique provides a route to extract ionic potentials of mean force that are not affected by the thermal fluctuations, which limits the accuracy of most past approaches including the popular umbrella sampling technique. © *2012 American Institute of Physics*. [http://dx.doi.org/10.1063/1.4753986]

I. INTRODUCTION

The behavior of ions at aqueous interfaces is relevant to a number of physicochemical processes, including atmospheric chemistry, electrochemistry, and self assembly of biomolecules and materials in solution. Understanding and predicting the ion distribution at interfaces is therefore of considerable interest. Both experiments and computer simulations have shown that the traditional image where ions are depleted from the interface is not entirely accurate.[1–3] Molecular dynamics simulations have shown that the iodide and bromide densities are enhanced at the water surface, whereas the fluoride anion is repelled from the surface and the chloride anion would feature an intermediate behavior. These observations are consistent with second harmonic generation and photoelectron spectroscopy experiments.[1] Recent vibrational sum frequency spectroscopy (VSFS) experiments[4] have suggested that the interfacial ions introduce very small perturbations in the water molecules located in the outermost layer. It was also concluded that the population of anions at the interface is reduced with respect to the bulk. The VSFS experiments have been revisited more recently using computer simulations. These simulations support ion enhancement at the interface, particularly of the larger anions.[5] At the same time, the simulations reproduced the experimental features of the vibrational spectra. This work has highlighted the relevance of intermolecular correlations in determining the experimental spectra.

Computer simulation studies have indicated that ion polarization is an important element in determining the ion enhancement at interfaces.[3,6,7] These studies have prompted the introduction of such polarization effects in Poisson-Boltzmann (PB) theories.[8] In these approximations water is modeled as a dielectric continuum, and the interface is represented through dielectric discontinuities, in the spirit of the Onsager and Samaras theory.[9] Hence, the molecular structure of interfacial water and the concomitant electrostatic potential of the bare water surface are neglected to a first approximation. We note that the magnitude of the water interfacial potential is still a subject of debate, as simulations and experiments disagree both in the sign and magnitude of the potential.[10] Recent computations using *ab initio*-density

a)Electronic mail: f.bresme@imperial.ac.uk.
b)Electronoic mail: echacon@icmm.csic.es.
c)Electronic mail: pedro.tarazona@uam.es.
d)Electronic mail: a.wynveen@gmail.com.

 © 2012 American Institute of Physics

Downloaded 12 Dec 2012 to 128.101.221.90. Redistribution subject to AIP license or copyright; see http://jcp.aip.org/about/rights_and_permissions

functional theory (AI-DFT) have also provided disparate results.[11,12]

The observation of a significant anion enhancement at the water surface has prompted a number of questions. In particular, how can the large enhancement be reconciled with the increase in surface tension measured in experiments when salt is added to the solution, since the surface tension increase would indicate a negative adsorption as predicted by the Gibbs adsorption isotherm (GAI). This issue has been recently discussed in theoretical and experimental works.[1,13] As noted by Petersen and Saykally,[1] however, the density enhancement of ions at the water surface is compatible with a negative adsorption, and therefore with the GAI, provided there is a depletion of ions in the layers next to the outermost surface.

Different ions feature different degrees of density enhancement at the interface. This species-dependent tendency of the ions to approach the water surface is a clear illustration of ion selectivity, which is epitomized by the Hofmeister series, which ranks ions according to their effect on the solubility of proteins.[14] At concentrations normally used to investigate Hofmeister effects, both ion-solvent electrostatic interactions and ion dispersion forces are expected to play a role in defining selectivity, as the ionic interactions are strongly screened.[15,16] Recent simulation work has also highlighted the role of solute polarizability on ion selectivity,[17] which must be relevant to understand Hofmeister effects. It was shown that the iodide modeled as a nonpolarizable ion features an enhancement in the density at the water solute interface. It was also found that lithium features a similar density enhancement, which is significantly increased by the solute polarizability. Unlike the halogen ions, lithium is not strongly polarizable, hence this result begs the question why it behaves in this way. The behavior observed for lithium is different to that observed using the Poisson Boltzmann theory, which indicated that alkali metal cations are depleted from the interfacial region[8] (however, we note that continuum theories and simulations can be corrected and explicit experimental information included to take into account the hydration of the ions near the surface[18,19]). We suggested in our previous work that the affinity of small cations such as lithium to the interfacial region might be driven by solvation effects, as this ion features a well-defined water solvation shell.[17] This observation, based on classical simulations, agrees with density functional *ab initio* computations,[20] and highlights the strong dependence of the solvation properties of monatomic ions with ion size. Indeed, recent computer simulations have convincingly shown a correlation between ion size/charge and ion selectivity.[21–27] Similarly, the sensitivity of the ion-ion potential of mean force to the force-field parameters had been noted previously,[28] and has been confirmed more recently,[17] indicating the subtle role that the ion size, and the dispersion interactions, have in determining the structure of aqueous interfaces.

In the great majority of previous simulation studies, the interfacial structure has been computed using mean density and mean orientational profiles. A notable exception is the work reported in Ref. 29, which made use of an intrinsic surface analysis to extract valuable information of the influence of the ions on the interfacial fluctuations. Because the mean density profiles are affected by thermal fluctuations, i.e., interfacial capillary waves, which smooth out the interfacial structure, it is quite possible to overlook interfacial ion enhancement, particularly if this enhancement is not very strong, or not as strong as the enhancement reported in the simulations of polarizable ions.[3] Recently, new algorithms have been introduced to investigate the *intrinsic* interfacial structure. These algorithms eliminate the averaging effect of thermal fluctuations.[30,31] This approach, and similar ones,[32–34] have been applied to a number of fluid interfaces; simple fluids,[35] water,[36,37] alkali fluids,[38] oil-water interfaces,[32,39–41] hydrophilic interfaces,[42] and molten salts.[43] The intrinsic profile offers a higher level of resolution of the interface, and, unlike the mean profiles, it is independent of the interfacial cross sectional area used in the simulations. Hence, these intrinsic density profiles provide a better reference to compare simulation data with experimental results obtained using spectroscopic techniques.[44] Moreover, it is possible to extract the intrinsic potential of mean force, again eliminating the smoothing effect of the capillary waves, which affects all the potential of mean force computations that have been performed thus far.

In this paper, we compute the *intrinsic* interfacial structure of aqueous solutions of alkali halides. The paper is structured as follows. First, we discuss the models and simulation methods employed in this work. A summary of the computational approach used to obtain the intrinsic profiles and the results from this analysis follows. We then present our results for the intrinsic density and orientational profiles, intrinsic potentials of mean forces, and electrostatic potential profiles. We close the paper with a section devoted to conclusions and further remarks.

II. METHODOLOGY

A. Model and simulation details

There are a number of issues associated with the simulation of ionic solutions. Point charge models have been extensively used in the past to investigate bulk and interfacial properties of water and aqueous solutions. Most of these models, including polarizable ones, have been fitted to reproduce bulk properties, hence they may ignore specific effects that may arise at interfaces. With regards to polarization, recent studies using polarizable models for water and ions have shown that these models tend to overpolarize both at interfacial and bulk conditions leading to an over prediction of ion adsorption (see, e.g., discussion in Ref. 45). Similarly, AI-DFT computations of water predict structural and coexistence properties that differ from those of experiment, highlighting the need for significant advances in the development of functionals that handle more accurately dispersive interactions.[46] In this paper, we employ point charge models. Given the wide range of studies performed with this approach, they provide a good starting point to address the main aim of this paper, namely, the computation of intrinsic interfacial structure, and to obtain a qualitative view of the structure of interfacial solutions for a wide range of salt conditions.

We have investigated aqueous solutions at two different concentrations: 1.0 m, where coulombic interactions are significantly screened, and 0.2 m, which is on the order of

Downloaded 12 Dec 2012 to 128.101.221.90. Redistribution subject to AIP license or copyright; see http://jcp.aip.org/about/rights_and_permissions

TABLE I. Lennard Jones parameters of the FF1 forcefield, from Dang, Garrett, and Smith;[51–54] adapted for the combining rules of σ and ϵ and water models used in these studies.[62]

Ion	σ (Å)	ϵ (kJ/mol)
Li^+	1.506	0.6904
Na^+	2.35	0.54392
K^+	3.332	0.4184
F^-	3.168	0.8368
Cl^-	4.401	0.4184
I^-	5.167	0.4184

physiological salt concentrations. The higher concentration range is relevant to investigations of the Hofmeister effects in biomolecules.[47–50] The ions are modeled as nonpolarizable Lennard-Jones (LJ) spheres using the parameters reported by Dang *et al.*[51–54] (see Table I.) Two of us have investigated extensively the performance of this force field (FF1) against other models in a recent publication.[17] Moreover, the performance of this model to reproduce the dielectric constant and osmotic pressure of aqueous solutions has been recently tested.[55] It was shown that the experimental decrease of the dielectric constant with salt concentration is very well reproduced, and the osmotic coefficient shows almost quantitative agreement with experiment for LiCl and KCl salts, while it is qualitative for other salts. Hence, we consider this force field a good starting point for our investigations.

Very recently, a new set of ion parameters has been derived for alkali halides.[56] This new force field (FF2) has been parametrized to reproduce the solution density at 293.15 K and 1 bar. Fitting to the solution density might be less sensitive to the solution composition than other properties (see above) at low concentrations. This reparametrization results in ion diameters that in extreme cases, e.g., Li^+ and I^-, can deviate significantly ($\sim$10%-20%) from the Dang *et al.* forcefield parameters. We also use the new parameters in FF2 to assess the sensitivity of the intrinsic profiles to the force field.

The LJ potential for ion-ion and ion-water interactions is defined as

$$u_{ij}(r) = 4\varepsilon_{ij}\left[\left(\frac{\sigma_{ij}}{r}\right)^{12} - \left(\frac{\sigma_{ij}}{r}\right)^{6}\right] - u_{ij}(r_c) \text{ for } r \le r_c, \quad (1)$$

$$u_{ij}(r) = 0 \text{ for } r > r_c, \quad (2)$$

where the cross interaction parameters between species i and j were obtained by standard combining rules, $\sigma_{ij} = \frac{1}{2}(\sigma_i + \sigma_j)$ and $\epsilon_{ij} = \sqrt{\epsilon_i \epsilon_j}$. The interactions were truncated and shifted at the cut-off distance, $r_c = 14$ Å. Water was modeled using the SPC/E water model.[57] We have shown that the intrinsic interfacial structure of this model is comparable to that predicted by more accurate four site models.[41] Although the SPC/E model is nonpolarizable, we consider this to be a good approximation, as previous simulations of water next to surfaces with markedly different polarizabilities essentially yield the same results regarding interfacial structure and electrostatic fields.[58,59] The long range electrostatic interactions arising from the charges in the ions and water atomic sites were computed using the particle mesh Ewald summation method.[60]

The interface simulations were performed using a liquid slab in a prismatic box, with typical dimensions $(L_x, L_y, L_z) = (30, 30, 300)$ Å. The lateral size was large enough to avoid problems associated with the use of periodic boundary conditions,[61] and the longitudinal dimension was chosen to minimize the correlation between the two water surfaces. The ions were randomly inserted in the water slab, which had been previously equilibrated for 10 ns. A further 10 ns was used for equilibration, and the simulations were run an additional 60 ns for the computation of the intrinsic profiles and thermodynamic properties. The equations of motion were integrated using the "leap frog" algorithm with a 2 fs time step. All the simulations were performed in the canonical (NVT) ensemble at $T = 298$ K using the Nosé-Hoover thermostat. A typical simulation consisted of 4300 water molecules and either 80 or 15 ion pairs, corresponding to the high and low concentration solutions respectively.

B. Intrinsic density profiles

The computation of the interfacial structure has witnessed important advances in the last years,[30–34,39,40] thanks to the development of novel algorithms that eliminate the blurring effect of capillary waves (CW). Simulations have shown that CW affect the profiles for relatively small simulation boxes.[61,63,64] The interfacial width follows the area dependence predicted by the capillary wave theory. In this work, we have used the so-called *intrinsic sampling method* (ISM),[30] to identify the water molecules belonging to the intrinsic surface. The resulting surface molecules were then used to construct a two dimensional surface,

$$\xi(\mathbf{R}, q_m) = \sum_{|\mathbf{q}|=2\pi/L_x}^{|\mathbf{q}|=q_m} \hat{\xi}_q \exp(i\,\mathbf{q}\cdot\mathbf{R}), \quad (3)$$

which is defined as the minimum area surface passing through the intrinsic surface molecular sites with coordinates $\mathbf{R} = (x, y)$, where $\mathbf{R}$ is defined by the center of mass coordinates in the water molecule. The intrinsic density profile is then defined as

$$\tilde{\rho}(z) = \left\langle \frac{1}{A_0} \sum_{i=1}^{N} \delta(z - z_i + \xi(\mathbf{R}_i)) \right\rangle, \quad (4)$$

where A_0 is the cross sectional area of the interface.

As shown in Eq. (3), the intrinsic surface depends on the parameter $q_m = 2\pi/\lambda_c$, where λ_c is the wavelength cut-off for the capillary wave spectrum. As discussed in previous work,[35] the optimum wavelength cut-off corresponds to one molecular diameter. The sharpest resolution of the intrinsic profile can be obtained by choosing $\lambda_c = \sigma_{H_2O} = 3.166$ Å, where σ_{H_2O} is the diameter of the oxygen site in the SPC/E model.

The intrinsic profiles were obtained from the analysis of $(6 - 8) \times 10^3$ uncorrelated configurations to ensure good sampling of the shortest wave vector, $|\mathbf{q}| = 2\pi/L_x$. The intrinsic surface was first computed using the center of mass position of the water molecules. Subsequently, the intrinsic

Downloaded 12 Dec 2012 to 128.101.221.90. Redistribution subject to AIP license or copyright; see http://jcp.aip.org/about/rights_and_permissions

density profiles for water and the ions were computed with respect to the intrinsic surface position.

The computations presented in this work correspond to an occupancy, i.e., number of pivots per unit area, of $n_s\sigma_{H_2O}^2 = 1.1$. This occupancy is the optimum one for the SPC/E water model because it leads to the sharpest resolution for the layering structure in the intrinsic density profile[36] and leads to a minimum in the rate of exchange of the pivots at the intrinsic surface.[35] We refer the reader to previous work[35] for a detailed discussion of this point.

In order to investigate the orientation of the interfacial water molecules, we use orientational intrinsic profiles. Again, we make use of the intrinsic surface as a reference to compute the orientational profile, therefore eliminating the thermal capillary wave fluctuations. The orientational profile was computed from

$$\tilde{p}(z) = \left\langle \sum_{i=1}^{N} \frac{\hat{\mathbf{p}}_\mathbf{i} \cdot \hat{\mathbf{z}}}{A_0} \delta(z - z_i + \xi(\mathbf{R}_i)) \right\rangle, \tag{5}$$

where $\hat{\mathbf{p}}_\mathbf{i}$ is the unitary vector pointing in the direction of the dipole moment of the water molecule i. Note that $\tilde{p}(z)$ is weighted by the corresponding water intrinsic density profile, so in order to obtain the average orientation of a water molecule we must divide $\tilde{p}(z)$ by the water intrinsic density profile $\tilde{\rho}(z)$.

In order to quantify the surface electrostatic potential, we have computed the intrinsic total electrostatic potential $\tilde{V}(z)$, i.e., the average electrostatic potential at distance z from the intrinsic surface. The usual mean total electrostatic potential,

$$V(z) = \frac{1}{\epsilon_0} \int_{-\infty}^{z} dz' \int_{-\infty}^{z'} \rho_c(z'')dz'', \tag{6}$$

can be computed from the mean total charge distribution, $\rho_c(z')$, including both the free charges and the partial charges in the water molecule. However, the intrinsic total electrostatic potential cannot be obtained from the intrinsic total charge distribution. So we have used

$$\tilde{V}(z) = \left\langle \frac{1}{A_0} \int \int d\mathbf{R} V(\mathbf{R}, z + \xi(\mathbf{R})) \right\rangle, \tag{7}$$

where the electrostatic potential $V(\mathbf{R}, z + \xi(\mathbf{R}))$ is evaluated using the same Ewald sum as that used in the molecular dynamics simulation. We note that the substitution of the charge density in Eq. (6) by the corresponding intrinsic charge density, does not lead to the same intrinsic potential. The result is similar to that obtained from Eq. (7) but not equal. Hence, we propose Eq. (7) as the correct approach to quantify the intrinsic electrostatic potential.

III. RESULTS

Figure 1 shows the mean density profiles for aqueous solutions of representative alkali halides at 1.0 m concentration. We recall that these profiles depend on the interfacial area employed in the simulations. The density shows the same features reported in previous works. For LiCl there is evidence for the formation of a double layer, with the cation approaching the water surface slightly more than the anion.

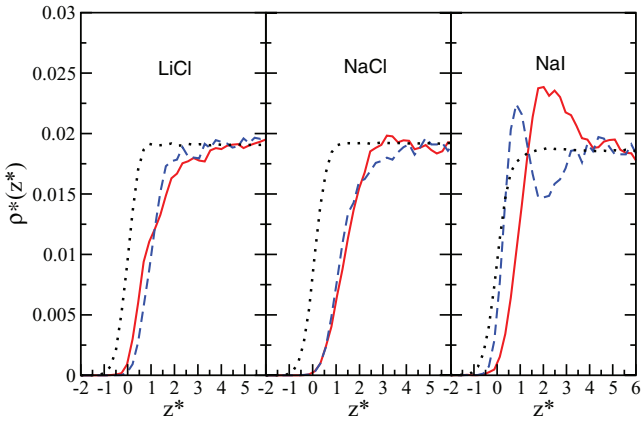

FIG. 1. Mean density profiles of aqueous solutions at 1.0 m concentration. The density profiles of water (dotted lines), cations (full lines), and anions (dashed lines) are shown. The density profile for water has been rescaled to facilitate its comparison with the ion density profiles. The density, $\rho^* = \rho\sigma_{H_2O}^3$, and the position, $z^* = z/\sigma_{H_2O}$, are represented in reduced units, where $\sigma_{H_2O} = 3.166$ Å is the effective diameter of the SPC/E water molecule.

For NaCl the double layer is reduced, and the density profiles for both ions almost fall on top of each other. For NaI, which includes the biggest anion investigated here, there is a clear evidence of charge ordering with respect to the interface plane, as revealed by the oscillatory behavior. As compared with the other salts, there is also a large enhancement of the anion density in the interfacial region. In line with previous observations,[24,25] there is no need to include explicit polarizability in the ionic models in order to achieve this density enhancement. This observation also agrees with earlier computer simulations of simple ionic liquids, consisting of mixtures containing two anions and a common cation. In that case, an enhancement of the larger ion at the liquid-vapor interface was also observed.[23] This effect is equivalent to the one observed in aqueous solutions investigated here and in other works.

The mean density profiles provide some insight into the interfacial structure but they hide important structural information. In particular, they do not fully resolve the ion distribution at the interface, which, as described below, is characterized by strong layering in the LiCl and NaCl cases as well. This structure is revealed by using the intrinsic sampling analysis.

A. Intrinsic density profiles

We start the discussion of the intrinsic structure by analyzing the impact that the addition of salt has on interfacial water. Figure 2 shows the intrinsic profiles for two of the salts presented in Figure 1. The intrinsic profile of water features a delta function peak that corresponds to the intrinsic surface, or liquid surface. This peak is followed, in the aqueous region, by a second peak at a distance of about one water molecular diameter from the surface. Beyond this second peak the profile is structureless, a feature that has been interpreted as characteristic of the low-coordinated structure of liquid water.[36] Interestingly, the addition of salt at the highest concentration considered here, 1.0 m, does not have a significant impact on

Downloaded 12 Dec 2012 to 128.101.221.90. Redistribution subject to AIP license or copyright; see http://jcp.aip.org/about/rights_and_permissions

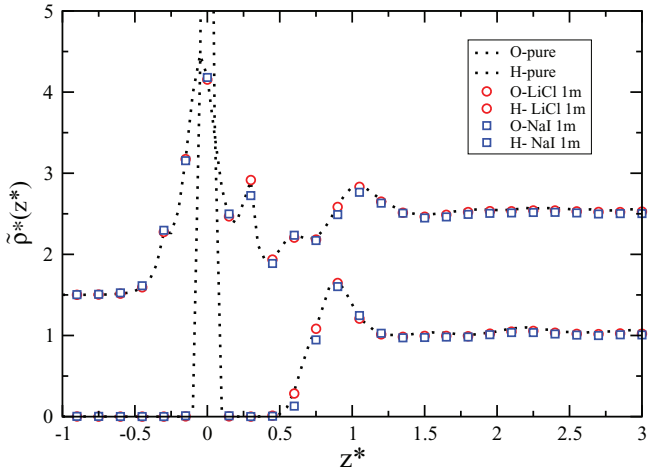

FIG. 2. Intrinsic density profile of water oxygen and hydrogen atoms (the latter has been shifted vertically 1.5 units) contributions. Pure water—dotted lines; LiCl 1.0 m solution—circles; NaI 1.0 m solution—squares.

the interfacial structure, not even in the arrangement of the hydrogen atoms belonging to molecules located at the intrinsic surface (see Figure 2). We will see below, by analyzing the orientational intrinsic profiles, that the ions do perturb the water orientational structure, but this perturbation varies greatly for the different salts considered here.

Figure 3 shows our results for the intrinsic profiles of alkali halide solutions as a function of salt composition and concentration. First of all the intrinsic profiles reveal a much richer structure. We can clearly identify now the peaks and depletion regions in the vicinity of the water surface. Our results for the (Li, Na, K)-Cl salts clearly show the large impact that the cation size has on the aqueous interfacial structure (see top-left panel in Figure 3). We find clear evidence of layering in all cases, with the cations and anions oscillating in antiphase for Li^+ and Na^+ salts. This layering disappears for the larger K^+ cation. The nature of the cations has little impact on the Cl^- profile, which is identical within the uncertainty of the simulation. This idea can be quantified through the intrinsic potential of mean force (IPMF), $\beta\tilde{W}(z^*) = -\ln\tilde{\rho}^*(z^*)$, (see top panel in Figure 4), which features small changes in the effective interactions of Cl^- with the cation species. Interestingly, the Cl^- intrinsic profile features a maximum at $\approx\sigma_{H_2O}$, which coincides with the maximum observed in the oxygen density profile, hence the density enhancement is relegated to the water subphase. We have estimated the amount of Cl^- anions, $n_{Cl,surf}$, that accumulate below the water surface, by integrating the intrinsic profile up to the first minimum. The ratio $n_{Cl,max}/n_{Cl,bulk}$, where $n_{Cl,bulk}$ is the number of Cl^- ions at the bulk concentration, 1.0 m, gives an indication of the amount of Cl^- accumulated in that interfacial region. We

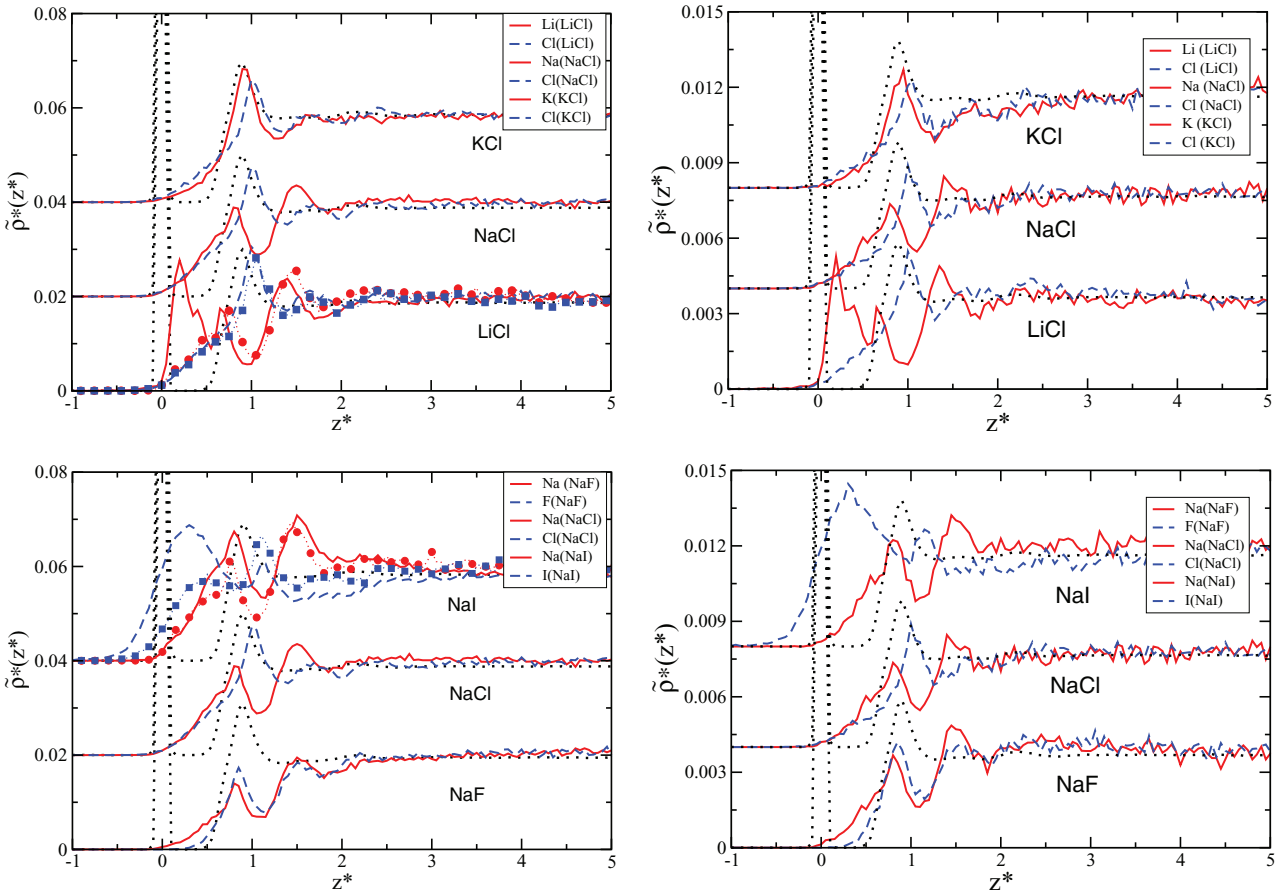

FIG. 3. Intrinsic density profiles of aqueous solutions at 1.0 m (left) and 0.2 m (right) concentrations. Dotted lines represent the intrinsic profile of the oxygen atoms in water. The profiles have been shifted vertically to facilitate the comparison of the different results. Full lines—cations and dashed lines—anions. The symbols correspond to an alternative force field (FF2)[56] for LiCl and NaI, where Li^+ and I^- have significantly larger and smaller diameters, respectively. Circles-cation; squares-anion. The density profile for water has been rescaled to facilitate its comparison with the ion intrinsic profiles.

Downloaded 12 Dec 2012 to 128.101.221.90. Redistribution subject to AIP license or copyright; see http://jcp.aip.org/about/rights_and_permissions

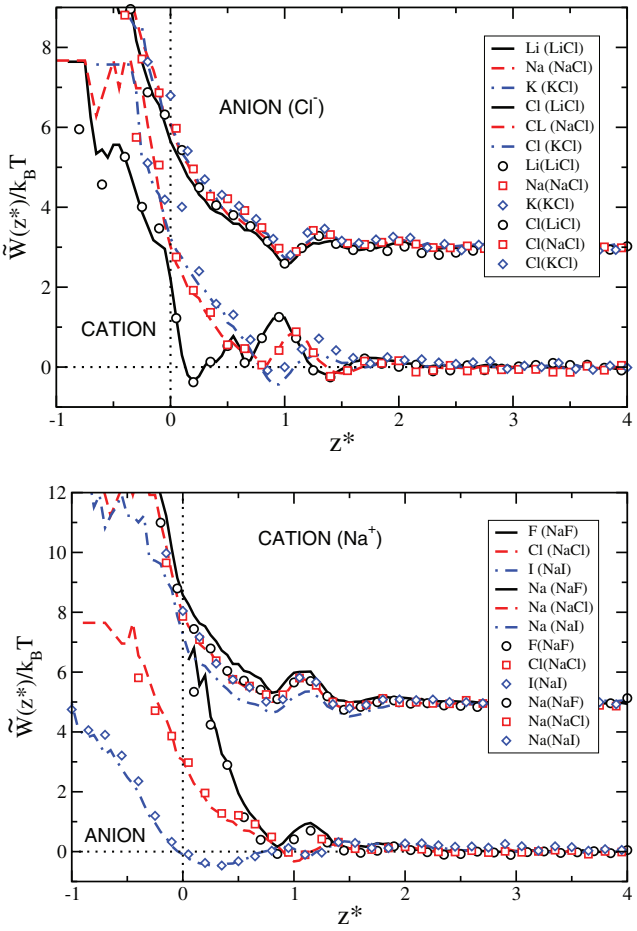

FIG. 4. The anion and cation intrinsic potential of mean force $\tilde{W}(z^*)$. (Top panel) dependence of $\tilde{W}(z^*)$ with the species of the cations for the anion partner Cl^-; (bottom panel) $\tilde{W}(z^*)$ for different anions but with the same cation partner Na^+. In the top panel, the anion curves have been shifted vertically 2.5 units, and in the bottom panel the cation curves have been shifted vertically 5 units. The lines represent the values for the 1.0 m solutions and the symbols for the 0.2 m solutions. All the results were obtained with the Dang *et al.* model discussed in the text.

find this amount is not much different from the one expected in bulk, $n_{Cl,max}/n_{Cl,bulk} = 1.17$ (LiCl), 1.03 (NaCl), and 0.98 (KCl). There is a weak dependence with the cation nature, with the smaller cation dragging more anions towards the interfacial region.

The larger impact of the Li^+ cation, which is particularly evident in the case of the Dang's model, can be understood by inspecting its intrinsic profile in more detail (see top-left panel in Figure 3). Li^+ features a prominent peak just below the water surface. These Li^+ ions act as a "bridge" between the water surface and the first water layer in the bulk aqueous phase. The density enhancement of Li^+ at the interface agrees with previous investigations of Li^+ cations near dielectric nanoparticles.[17] In that work we showed that, for the Dang *et al.* force field, the Li^+ cations are tightly solvated by four water molecules arranged in a tetrahedral structure. This solvation structure is very robust, and it is preserved right at the interface with the nanoparticle. The tetrahedral coordination agrees with *ab initio* density functional theory computations.[20,65,66] The coordination number estimated using neutron diffraction experiments of "deuterated" water is slightly larger though, 6.5 ± 1, at 1.0 m concentration.[67] Both classical and *ab initio* computations predict LiO distances of 1.96 Å, in good agreement with neutron scattering experiments, and LiH distances of 2.64 Å, about 10% larger than the LiD distance reported in experiments.[67] These cation-water distances are fairly insensitive to the salt concentrations investigated here, which also agree with experiments. We note that the lithium peak observed in the Dang's model is very sensitive to ion size, as shown in the results obtained with the FF2 model, which consider a larger diameter for the lithium ion (see Figure 3, top left). The LiO distance predicted by the FF2 model, 2.19 Å, is nonetheless longer than that obtained with Dang's model, AI-DFT computations and neutron scattering results.

Our results for Li^+ contrast with the result expected from the classical electrostatic approach to electrolyte solutions at interfaces, which is based on constructing a dielectric boundary that separates two homogeneous media with different dielectric constants, 1 for the vapor and 78 for water. The image charge approach is implemented to consider the interactions arising from this dielectric discontinuity. Following this approach one would expect that the ions are depleted from the interface. Clearly, Li^+ does not follow this idea, a notion that has been noted before in earlier studies.[17,27] The behavior we observe here for Li^+ is driven by water solvation, showing that the explicit consideration of the solvent is essential to define the ionic interfacial density. Such effects cannot be reproduced using continuum solvent models except, possibly, by artificially increasing the effective ion diameter.

The peculiar shape of the peak centered about $z^* \approx 0.25$ in the Li^+ intrinsic profile can be traced back to the tetrahedral structure mentioned above. In Ref. 17, we showed that $[Li(H_2O)_4]^+$ was arranged such that the three water molecules, forming one base of a pyramid, are located at the interface, while the remaining water molecule was deeper in the bulk. Considering this orientation for the cluster, i.e., assuming that the three molecules forming the base of the pyramid are part of the intrinsic surface, and considering a Li^+–O distance projected on the direction normal to the interface, $R^*_{LiO,z} = 0.62$ Å, we find that a peak in the Li^+ density should be observed at $z^* \approx 0.2$. This estimate is in very good agreement with the main peak observed in the intrinsic profile (see Figure 3 top-left panel). The secondary peak observed in the profile, $z^* \approx 0.66$ is close to the LiO distance, indicating the preference for another conformation where one of the water molecules would be part of the intrinsic surface and the base of the pyramid formed by the other three molecules would lie deeper in the bulk region. These distinctive structural features are reflected in the intrinsic potential of mean force (IPMF) (see Figure 4 top panel), which features a minimum next to the intrinsic surface of $\approx -0.4 k_B T$ and an energy barrier of $\approx 1.3 k_B T$ at $z^* = 1$. This IPMF differs from the ones obtained from umbrella sampling approaches,[27] as the latter are affected by the ubiquitous thermal fluctuations, which result in a monotonic decay for the PMF with distance instead. As shown above, the lack of structural detail in the density profiles and potentials of mean force can be easily overcome using an intrinsic sampling calculation.

Downloaded 12 Dec 2012 to 128.101.221.90. Redistribution subject to AIP license or copyright; see http://jcp.aip.org/about/rights_and_permissions

Following the trends reported above for the cations, the intrinsic profiles for the anions exhibit a strong dependence with the anion diameter (Figure 3 bottom-left panel for results at 1.0 m concentration). With increasing size, the anion approaches the water surface to a greater extent. Iodide modeled with the Dang *et al.* model represents an extreme case in this instance, as the ions actually adsorb at the water surface (notice the tail in the intrinsic profile for $z^* < 0$ in the vapor region). This observation is in line with previous studies using rigid ion models[24,25] and shows again that polarization is not essential to enhance the interfacial density, although polarization contributes to increased ion adsorption. Of all the anions investigated here, I^- is also the one that results in stronger layering and charge oscillation, which is significant at distances up to ~2-3 σ_{H_2O} units from the water surface. I^- also influences the interfacial structure of Na^+, whose density follows the I^- density and oscillates in antiphase. This qualitative behavior is reproduced by the FF2 model, which predicts a weaker adsorption of I^- at the interface (see Figure 3 bottom- left). The importance of the anion size is more evident in the potentials of mean force (see Figure 4 bottom panel). The IPMFs clearly show that the affinity of the anions to approach the interface increases with their diameter, F^- <Cl^- <I^-, with the I^- IPMF featuring a minimum of $\approx -0.5 k_B T$. We find that the IPMF of the Na^+ counterion is modified slightly by the nature of the anion. Our results for the IPMFs are consistent with previous estimates based on computations using a constrained mean force approach, which reported a stronger affinity for the larger anion, I^-, to approach the surface.[6]

We have also analyzed the impact of the salt concentration on the intrinsic profiles and the potentials of mean force (see Figure 3 right-top and bottom panels, and Figure 4 top and bottom panels). At physiological relevant concentrations, 0.2 m, the interfacial ion structure is essentially the same as that at 1.0 m, except for the obvious change in the average bulk concentration. This is surprising considering the change in the Debye length. The insensitivity of the ion structuring to concentration in the range 0.2-1.0 m is also reflected in the IPMFs, where the 0.2 m results essentially follow the data at the higher concentration.

B. Intrinsic water orientation

Figure 5 (top and bottom) shows the orientation profiles at two different concentrations. We find that, in the 0.2-1.0 m range, the salt concentration does not significantly influence the intrinsic orientation profile of pure water. As shown in earlier work,[36] the intrinsic profiles indicate that water molecules adopt a preferred orientation. The dipole of the water molecules lying on the outer part of the water surface point towards the vapor phase, and the ones lying in the inner part point towards the aqueous (bulk) phase. The dipole moment of the water molecules located at one molecular diameter from the water surface points again towards the vapor region. Hence, the orientational structure is characterized by alternating layers of dipoles with a weak preference to point either towards the vapor or liquid regions. A similar conclusion can be inferred from the analysis of orientational profiles of water at liquid-liquid interfaces,[39] where the orientation profile is essentially the same as that of the free surface.

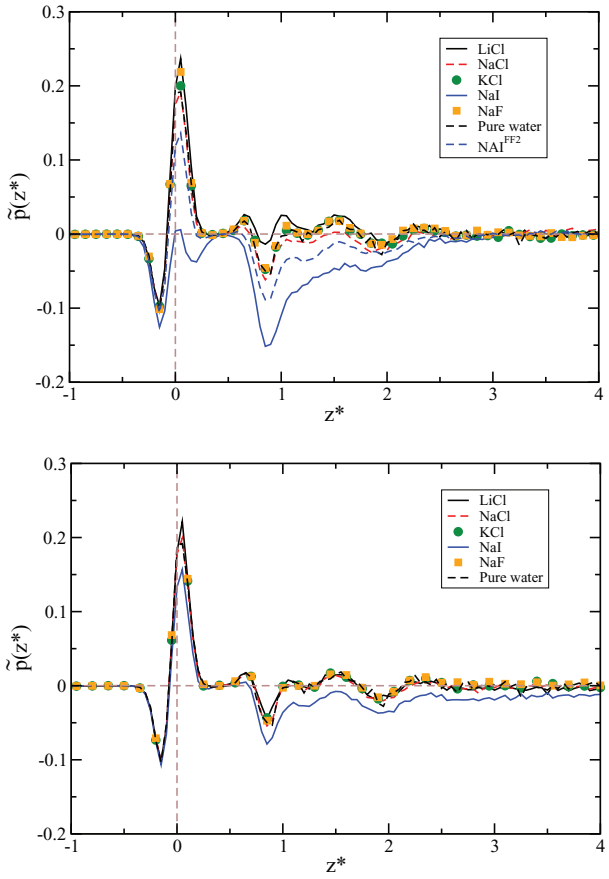

FIG. 5. Intrinsic orientational profiles of the water molecules for 1.0 m (top) and 0.2 m (bottom) concentrations. All the data were obtained with the parameters listed in Table I except for the FF2 case, where we used the parameters listed in Ref. 56.

For ionic salts, in particular, the small effect that the ions have on the water orientation is in broad agreement with experimental observations. Non-resonant second harmonic generation spectroscopy experiments indicate that the changes of the water orientation with salt are fairly minor up to 1.0 m concentrations, the differences between salt and pure water being within the uncertainty of the experiments.[68]

These small changes are compatible with our simulation data, except for I^-, which show a marked influence on the orientation of the water molecules. It is noticeable that the force field of Dang *et al.*, which assigns to I^- a large diameter ~5.17 Å, cancels the orientation of the water molecules at the water surface, but induces a strong orientation in the water subphase with the dipoles pointing towards the vapor. The orientation of the water dipole toward the interface at $\sim \sigma_{H_2O}$ is due to the water molecules solvating the iodide at the interface. The orientational order extends significantly inside the aqueous region, $\sim 3\sigma_{H_2O}$ units. The strong effect of the I^- ions is clear by inspecting the solution at lower concentration (see Figure 5 bottom) where the orientational distortion is significantly reduced. As with the intrinsic profiles, one may suspect that the strength of the distortion is most likely connected to the ion size, and the strong adsorption associated with this

Downloaded 12 Dec 2012 to 128.101.221.90. Redistribution subject to AIP license or copyright; see http://jcp.aip.org/about/rights_and_permissions

size. The analysis of the orientational profile using the second force field investigated in this work (FF2), which defines a smaller I^- diameter, 4.78 Å, (see above for discussion of the models), confirms this point. With the reduction of the ion diameter, we recover the characteristic orientational structure of the pure water surface, featuring two layers of molecules with opposite orientations. This change in orientation is consistent with the fact that for the second force field there are fewer iodides adsorbed at the interface. Other features are nonetheless preserved, in particular the enhanced orientation of the water molecules at $\sim \sigma_{H_2O}$ from the water surface. Because this effect appears in a wide range of ion sizes we conclude it must be representative of I^- in real ionic solutions. Indeed the effect that I^- has on the interfacial water structure has been highlighted in sum frequency spectroscopy experimental studies,[69] which indicate that this anion orients, on average, the dipoles of the interfacial water molecules towards the vapor phase.

C. Intrinsic electrostatic potential

Finally, we analyze the electrostatic potential of the aqueous solution interface. Experimental studies have reported a linear shift of the electrostatic potential with concentration.[70] The increase of the potential is proportional to the salt concentration. However, we note that there is still disagreement between experiments and simulations in the sign and absolute magnitude of the electrostatic potential of water.[11,12,71–73] The electrostatic potential computed in most AI-DFT studies provides information that is relevant for electron probes (see Refs. 73 and 74), hence this electrostatic potential is different from the ones computed in classical simulations of point charges (see Ref. 45). We note that other definitions of the *ab initio* electrostatic potentials are also possible.[74] One of the definitions is based on the *deformation charge potential*, which results in values that are negative and of the order of the ones found in classical simulations.[73] As we are interested in quantifying the changes in the electrostatic potential via the intrinsic sampling method, we have chosen here the standard approach employed in classical simulations of point charge models.

This approach has been widely used before, and it has been shown that both the concentration and salt composition effects are well reproduced by simulation models, and even the potential shifts are predicted at a quantitative level.[7] The shift of the electrostatic potential is associated with the different affinity of cations and anions to be near the water surface. Hence, this effect cannot be reproduced with primitive models employed in classical theories, which assume the same size for cations and anions.

To analyze the potential, we have chosen the highest concentration used here, 1.0 m. We note that even at this concentration the potential shifts reported in experiments and other simulations[25] are small, hence we focus our discussion on the intrinsic structure of the electrostatic potential and its magnitude in the interfacial region. The potential was computed following the method discussed in Sec. II B in combination with the intrinsic sampling method to eliminate the smearing effect of the thermal capillary waves. The electrostatic potential shows a structure that is inaccessible in many of the previous computational investigations of this quantity. The interfacial potential shows a strong oscillatory structure before reaching a stable value in the bulk region, $\sim 1.5\sigma_{H_2O}$, units from the water surface. Interestingly, the electrostatic potential associated with the water surface is much stronger than what can be inferred from the analysis of the average profiles. We find that it reaches a negative value ~4 times its value in bulk. At 1.0 m concentration, our results for the electrostatic potential are fairly insensitive to the salt composition, hence it is not possible to draw any conclusions from the electrostatic potential shift. Nonetheless, the insensitivity of the potential to salt is the result of a balance between the electrostatic potential due to the salt and the compensation of this potential by the water contribution, which depends on how the water restructures for the specific salt species. This idea has been discussed before in experiments[70] and computer simulations.[7] Weiss *et al.* presented a particularly detailed analysis based on molecular dynamics simulations.[25]

We have thus computed the salt contribution to the intrinsic electrostatic potential for different chloride and sodium salts investigated in this work, namely (Li,Na,K)Cl and NaI. Our results show a clear contribution of the salt to the potential (see Figure 6), except at the intrinsic surface,

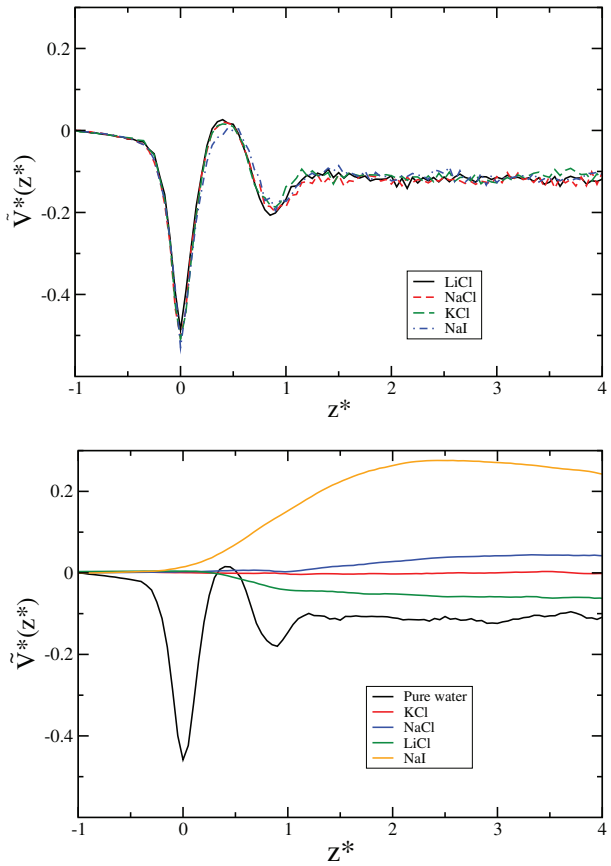

FIG. 6. Intrinsic interfacial electrostatic potential of electrolyte solutions at 1 m concentration. Top—total electrostatic potential. Bottom—salt contribution. All the results were obtained with the force-field parameters given in Table I (FF1). The electrostatic potential is represented in reduced units, $\tilde{V}^* = V 4\pi\epsilon_0\sigma_{H_2O}/e$, where e is the electron charge. 1 Volt corresponds to 0.2199 in reduced units.

Downloaded 12 Dec 2012 to 128.101.221.90. Redistribution subject to AIP license or copyright; see http://jcp.aip.org/about/rights_and_permissions

$z^* = 0$, where the effect is very small (NaI) or negligible ((Li,Na,K)Cl). For LiCl the contribution in the bulk is negative, meaning that the potential due to water must be more positive than that for pure water in order to compensate this extra negative contribution. This can be understood by considering the separation of the Li^+ and Cl^- at the interface, with Li^+ closer to the surface than Cl^-. This charge separation leads to an electric field pointing toward the bulk, giving a lower potential in the bulk as compared to that at the interface. Water is polarized as a response to the extent that the overall potential remains essentially unchanged within the accuracy of our simulations. For other salts, NaCl and NaI, we find that the ion electrostatic potential is positive, indicating the water contribution has to be more negative in comparison with that of pure water. The contribution from KCl is essentially zero, which is consistent with the small charge separation inferred from the intrinsic density profiles (see Figure 3 top left).

IV. CONCLUSIONS AND FINAL REMARKS

We reported the intrinsic interfacial structure of ionic solution of alkali halides by analyzing molecular dynamics simulations of rigid models with the intrinsic sampling analysis (ISA), which removes the averaging effect of the capillary waves on the density profiles.

The main conclusions from this work are given below.

Our results confirm that continuum theories such as Poisson Boltzmann cannot predict the interfacial characteristics of the different alkali halide salts. Namely, PB will not predict iodide and lithium density enhancement at the liquid-vapor interface. However, as illustrated in recent works, this continuum theory can be corrected by including experimental information to take into account the hydration of the ions at the interface. The ISA shows iodide adsorption following previous studies of rigid ions, and reveals a greater structure and enhanced adsorption for iodide than that reported in previous investigations. Furthermore, the ISA reveals a lithium peak near the interface, which may have been overlooked in other studies being this peak has been obscured by smearing at the interface due to thermal capillary waves, which are taken into account using the intrinsic method.

The tendency of the iodide and lithium to approach the interface is not only manifested by their distributions, but is also revealed by (i) the corresponding potentials of mean force, for which minima exist near or at the interface for both ions (as compared to a fully repulsive potential of mean force which is predicted by mean field theories that incorporate image charges due to the dielectric discontinuity at the interface), and (ii) the effect of the ionic distributions at the interface on the orientation of the dipolar moments of water at the interface.

Although both iodide and lithium modelled as point charges tend to approach the interface more so than the other cations and anions, the individual mechanisms underlying the behavior for these two ions are rather different. Iodide, having a very small solvation energy because of its large size (without even taking into account its polarization), will adsorb at the interface so as to not disrupt the bulk water structure, i.e., the chemical potential of water molecules in bulk water is more negative than that of iodide in bulk water. Furthermore, being there is an excess of water hydrogen to bond at the interface, the interfacial location of iodide is energetically favorable being it still can be solvated by the water hydrogen. Within the point charge approximation and using one of the models investigated here, lithium, on the other hand, abuts the first interfacial layer. Because of lithium's small size and positive charge, the natural water structure at the interface is commensurate with the tetrahedral organization of the solvating water about lithium. Indeed, lithium acts as a bridge between the interfacial water layer and the first interior water layer. Small changes in the cation diameter modify the water solvation structure and the tendency of the ion to approach the interface.

Even with the different ion-specific distributions of electrolyte at the interface, the electrostatic potential of a solution demonstrates a robust profile that appears to be independent of the salt species. The magnitude of the electrostatic potential at the water surface is about 4 times stronger than the one in bulk. The physical origin of this potential lies in the strong orientation of the water molecules at the outermost surface. Any distribution of ions is compensated by a restructuring and/or reorienting of the water at the interface so as to yield both interfacial and bulk potential profiles of the electrolyte systems that are nearly identical to that of pure water for concentrations up to 1 m.

The distributions of the ions, as seen using the ISA, demonstrate trends which may be predicted by the Hofmeister series. The latter describes how protein solubility increases in salt solutions composed of larger anions and smaller cations. Granted, many previous explanations of the Hofmeister series concern the effect of the changing surface tension of water with salt species, i.e., salts which increase surface tension lead to more hydrophobic behavior of the proteins and thus reduce their solubility and vice-versa. However, Hofmeister effects may result from direct electrolyte ion-protein interactions. Those ions that go to the liquid-vapor interface, such as iodide and possibly lithium, would also tend to approach the protein surface, according to the mechanisms described above. This increased interaction between these electrolyte ions and the protein would increase the latter's solubility.

We note, however, that the interfacial ionic structure is very sensitive to the ion size, as reflected by the different results obtained with different force fields. The results presented in this work should provide a qualitative view of the structural changes expected in ionic solutions upon modifying the cation and/or anion size. Given the sensitivity of the ion distribution to ion size, it is clear that more work is needed to develop force fields that accurately represent the ion effective diameter.

Overall, the intrinsic sampling approach reveals ionic structure at water liquid-vapor interfaces that had been hitherto inaccessible in previous experimental and simulation studies. The latter are limited due to the smearing effects of thermal fluctuations/capillary waves at the interface. In order to see similar effects using mean field theories, these necessarily must be adapted to include solvation effects and the water structural properties at the interface described in this work.

Downloaded 12 Dec 2012 to 128.101.221.90. Redistribution subject to AIP license or copyright; see http://jcp.aip.org/about/rights_and_permissions

ACKNOWLEDGMENTS

We would like to acknowledge the Imperial College High Performance Computing Service for providing computational resources. Financial support for this work was provided by The Royal Society and the Dirección General de Investigación, Ministerio de Ciencia y Tecnología of Spain, under Grant No. FIS2010-22047-C05, and by the Comunidad Autónoma de Madrid under the R&D Program of activities MODELICO-CM/S2009ESP-1691. F.B. would like to thank the EPSRC for the award of a Leadership Fellowship.

[1]P. B. Petersen and R. J. Saykally, Annu. Rev. Phys. Chem. **57**, 333 (2006).
[2]P. Jungwirth and D. J. Tobias, J. Phys. Chem. B **106**, 6361 (2002).
[3]P. Jungwirth and D. J. Tobias, Chem. Rev. **106**, 1259 (2006).
[4]E. Raymond and G. Richmond, J. Phys. Chem. B **108**, 5051 (2004).
[5]T. Ishiyama and A. Morita, J. Phys. Chem. C **111**, 738 (2007).
[6]L. Dang, J. Phys. Chem. B **106**, 10388 (2002).
[7]T. Ishiyama and A. Morita, J. Phys. Chem. C **111**, 721 (2007).
[8]Y. Levin, Phys. Rev. Lett. **102**, 147803 (2009).
[9]L. Onsager and N. N. T. Samaras, J. Chem. Phys. **2**, 528 (1934).
[10]V. Sokhan and D. Tildesley, Mol. Phys. **92**, 625 (1997).
[11]S. Kathmann, I. Kuo, and C. Mundy, J. Am. Chem. Soc. **131**, 17522 (2009).
[12]K. Leung, J. Phys. Chem. Lett. **1**, 496 (2010).
[13]Y. Levin, A. dos Santos, and A. Diehl, Phys. Rev. Lett. **103**, 257802 (2009).
[14]F. Hofmeister, Arch. Exp. Pathol. Pharmakol **24**, 247 (1888).
[15]M. Boström, D. R. M. Williams, and B. W. Ninham, Phys. Rev. Lett. **87**, 168103 (2001).
[16]W. Kunz, P. L. Nostro, and B. Ninham, Curr. Opin. Colloid Interface Sci. **9**, 1 (2004).
[17]A. Wynveen and F. Bresme, J. Chem. Phys. **133**, 144706 (2010).
[18]A. dos Santos, A. Diehl, and Y. Levin, Langmuir **26**, 10778 (2010).
[19]A. Diehl, A. dos Santos, and Y. Levin, J. Phys.: Condens. Matter **24**, 284115 (2012).
[20]A. Lyubartev, K. Laasonen, and A. Laaksonen, J. Chem. Phys. **114**, 3120 (2001).
[21]J. Abascal, F. Bresme, and P. Turq, Mol. Phys. **81**, 143 (1994).
[22]B. Schnell, R. Schurhammer, and G. Wipff, J. Phys. Chem. B **108**, 2285 (2004).
[23]F. Bresme, M. Gonzalez-Melchor, and J. Alejandre, J. Phys.: Condens. Matter **17**, S3301 (2005).
[24]B. Eggimann and J. Siepmann, J. Phys. Chem. C **112**, 210 (2008).
[25]D. J. V. A. dos Santos, F. Müller-Plathe, and V. C. Weiss, J. Phys. Chem. C **112**, 19431 (2008).
[26]I. Kalcher, D. Horinek, R. Netz, and J. Dzubiella, J. Phys.: Condens. Matter **21**, 424108 (2009).
[27]D. Horinek, A. Herz, L. Vrbka, F. Sedlmeier, S. Mamatkulov, and R. R. Netz, Chem. Phys. Lett. **479**, 173 (2009).
[28]L. Dang, B. Pettitt, and P. Rossky, J. Chem. Phys. **96**, 4046 (1992).
[29]D. Otten, P. Shaffer, P. Geissler, and R. Saykally, Proc. Natl. Acad. Sci. U.S.A. **109**, 701 (2012).
[30]E. Chacón and P. Tarazona, Phys. Rev. Lett. **91**, 166103 (2003).
[31]P. Tarazona and E. Chacón, Phys. Rev. B **70**, 235407 (2004).
[32]J. Chowdhary and B. Ladanyi, J. Phys. Chem. B **110**, 15442 (2006).
[33]L. Partay, G. Hantal, P. Jedlovszky, A. Vincze, and G. Horvai, J. Comput. Chem. **29**, 945 (2008).
[34]M. Jorge, P. Jedlovszky, and N. Cordeiro, J. Phys. Chem. C **114**, 20291 (2010).
[35]E. Chacón, M. Fernández, D. Duque, R. Delgado-Buscalioni, and P. Tarazona, Phys. Rev. B **80**, 195403 (2009).
[36]E. Chacón, P. Tarazona, and J. Alejandre, J. Chem. Phys. **125**, 014709 (2006).
[37]A. Willard and D. Chandler, J. Phys. Chem. B **114**, 1954 (2010).
[38]E. Chacón, P. Tarazona, and L. González, Phys. Rev. B **125**, 224201 (2006).
[39]F. Bresme, E. Chacón, P. Tarazona, and K. Tay, Phys. Rev. Lett. **101**, 056102 (2008).
[40]F. Bresme, E. Chacón, and P. Tarazona, Phys. Chem. Chem. Phys. **10**, 4704 (2008).
[41]F. Bresme, E. Chacón, and P. Tarazona, Mol. Phys. **108**, 1887 (2010).
[42]F. Bresme, E. Chacón, H. Martínez, and P. Tarazona, J. Chem. Phys. **134**, 214701 (2011).
[43]P. Tarazona, E. Chacón, and F. Bresme, J. Phys.: Condens. Matter **24**, 284123 (2012).
[44]P. B. Petersen and R. J. Saykally, J. Phys. Chem. B **110**, 14060 (2006).
[45]M. Baer, A. Stern, Y. Levin, D. Tobias, and C. Mundy, J. Phys. Chem. Lett. **3**, 1565 (2012).
[46]J. Wang, G. Roman-Perez, J. Soler, and E. Artacho, J. Chem. Phys. **134**, 024516 (2011).
[47]T. Arakawa and S. N. Timasheff, Biochemistry **21**, 6525 (1982).
[48]M. G. Cacace, E. M. Landau, and J. J. Ramsden, Q. Rev. Biophys. **30**, 241 (1997).
[49]E. Kokkoli and C. F. Zukoski, Langmuir **14**, 1189 (1998).
[50]J. W. Kurutz and S. H. Xu, Langmuir **17**, 7323 (2001).
[51]L. X. Dang, J. Chem. Phys. **96**, 6970 (1992).
[52]L. X. Dang and B. C. Garrett, J. Chem. Phys. **99**, 2972 (1993).
[53]D. E. Smith and L. X. Dang, J. Chem. Phys. **100**, 3757 (1994).
[54]L. X. Dang, J. Am. Chem. Soc. **117**, 6954 (1995).
[55]I. Kalcher and J. Dzubiella, J. Chem. Phys. **130**, 134507 (2009).
[56]S. Deublein, J. Vrabec, and H. Hasse, J. Chem. Phys. **136**, 084501 (2012).
[57]H. Berendsen, J. Grigera, and T. Straatsma, J. Phys. Chem. **91**, 6269 (1987).
[58]A. Wallqvist, Chem. Phys. Lett. **165**, 437 (1990).
[59]A. Kohlmeyer, W. Witschel, and E. Spohr, Chem. Phys. **213**, 211 (1996).
[60]T. Darden, D. York, and L. Pedersen, J. Chem. Phys. **98**, 10089 (1993).
[61]M. González-Melchor, F. Bresme, and J. Alejandre, J. Chem. Phys. **122**, 104710 (2005).
[62]I. S. Joung and T. E. Cheatham III, J. Phys. Chem. B **112**, 9020 (2008).
[63]D. Lacasse, G. Grest, and A. Levine, Phys. Rev. Lett. **90**, 309 (1998).
[64]S. Senapati and M. Berkowitz, Phys. Rev. Lett. **87**, 176101 (2004).
[65]A. Tongraar, K. Ledl, and B. Rode, Chem. Phys. Lett. **286**, 56 (1998).
[66]H. Loeffler and B. Rode, J. Chem. Phys. **117**, 110 (2002).
[67]I. Howell and G. Neilson, J. Phys.: Condens. Matter **8**, 4455 (1996).
[68]H. Bian, R. Feng, and H. Wang, J. Chem. Phys. **130**, 134709 (2009).
[69]N. Ji, V. Ostroverkhov, C. Tian, and Y. Shen, Phys. Rev. Lett. **100**, 096102 (2008).
[70]N. Jarvis and M. Scheiman, J. Phys. Chem. **72**, 74 (1968).
[71]M. Paluch, Adv. Colloid Interface Sci. **84**, 27 (2000).
[72]C. Barraclough, P. McTigue, and Y. Ng, J. Electroanal. Chem. **329**, 9 (1992).
[73]F. Bresme and E. Artacho, J. Math. Chem. **20**, 10351 (2010).
[74]S. Kathmann, I.-F. Kuo, C. J. Mundy, and G. Schenter, J. Phys. Chem. B **115**, 4369 (2011).

Downloaded 12 Dec 2012 to 128.101.221.90. Redistribution subject to AIP license or copyright; see http://jcp.aip.org/about/rights_and_permissions